Nonspecific-Adsorption Behavior of Polyethylenglycol and Bovine Serum Albumin Studied by 55-MHz Wireless-Electrodeless Quartz Crystal Microbalance

Hirotsugu Ogi[a,b], Yuji Fukunishi[a], Hiraonao Nagai[a],

Ken Okamoto[a], Masahiko Hirao[a], Masayoshi Nishiyama[c]

[a] *Graduate School of Engineering Science, Osaka University*

Machikaneyama 1-3, Toyonaka, Osaka 560-8531, Japan

[b] *PRESTO, JST, 4-1-8 Honcho, Kawaguchi, Saitama, Japan*

[c] *Central Workshop, Osaka University*

Machikaneyama 1-2, Toyonaka, Osaka 560-0043, Japan

Abstract

The nonspecific binding ability of polyethylenglycol (PEG) and bovine serum albumin (BSA) on modified and unmodified surfaces is quantitatively studied by a wireless-electrodeless quartz crystal microbalance (WE-QCM). PEG and BSA are important blocking materials in biosensors, but their affinities for proteins and uncoated substrates have not been known quantitatively. The WE-QCM allows quantitative analysis of the adsorption behavior of proteins on the electrodeless surfaces. Affinities of PEG, BSA, human immunoglobulin G (hIgG), and Staphylococcus protein A (SPA) for α-SiO_2 (quartz), Au thin film, PEG, and BSA are systematically studied by the homebuilt flow-injection system. PEG shows low affinities for

the SiO_2 surface (K_A=4.2×10^4 M^{-1}) and the Au surface (K_A=6.6×10^4 M^{-1}), but BSA shows higher affinity for the SiO_2 surface (K_A=1.4×10^6 M^{-1}). Both PEG and BSA show low affinities for hIgG (K_A ∼1.5×10^5 M^{-1}). However, the number of binding sites of PEG to hIgG is significantly larger than that of BSA, indicating that blocking for hIgG is favorably achieved by BSA, rather than PEG.

Key words: nonspecific adsorption, affinity, electrodeless, QCM

1 Introduction

Nonspecific adsorption of biomolecules has always caused troublesome problems in quantitatively measuring the concentration of a target protein and evaluating the binding affinity between proteins. This is especially important issue in the label-free biosensors such as quartz-crystal microbalance (QCM) and surface plasmon resonance (SPR) methods, because changes in the physical properties they detect are assumed to be caused by the specific adsorption between the receptor immobilized on the sensor surface and the target analyte. The nonspecific adsorption of the target molecule causes the overestimation of the affinity value. Thus, the blocking procedure has been indispensable in fabricating biosensor chips to avoid the nonspecific adsorption of analyte. Polyethylenglycol (PEG) (Senaratne *et al.* (2006); Shen *et al.* (2007); Shu *et al.* (2008); Drouvalakis *et al.* (2008)) and bovine serum albumin (BSA) (Wąsowicz *et al.* (2008); Suprun *et al.* (2008)) are widely used as important blocking materials because they are believed to show low affinities for antibodies and on unmodified surfaces. However, their nonspecific binding abilities have not been quantitatively investigated. Here, we determine the binding affinity among PEG, BSA, human immunoglobulin G (hIgG), Staphylococ-

cus protein A (SPA), α-SiO_2 (quartz) surface, and Au surface using the high sensitive wireless-electrodeless QCM (WE-QCM).

QCM is a label-free biosensor, allowing the quantitative monitoring of recognition behavior among biochemical molecules through changes in the resonance frequency of a quartz plate. Target molecules are adsorbed on the surface-modified quartz oscillator, resulting in the decrease in the resonance frequency (Sauerbrey (1959)). The resonance frequency can be monitored during association and dissociation reactions in real time without any labeling, yielding thermodynamic binding constants (Eddowes (1987); Ebara *et al.* (1996); Liu *et al.* (2003a,b)). It has been therefore a powerful tool for studying interactions among various biomolecules (Muramatsu *et al.* (1987); Liu *et al.* (2003a,b); Wang and Muthuswamy (2009); Edvardsson *et al.* (2009); Kang and Muramatsu (2009)).

We have recently achieved a significant breakthrough in QCM by developing the WE-QCM, which avoids the deterioration of the QCM sensitivity caused by deposited metallic electrodes and attached wires on the quartz surfaces (Ogi *et al.* (2006a, 2007a,b, 2008a,b)). The WE-QCM provides higher sensitivity because of the higher frequency measurements and then more reliable information on the biochemical reactions than conventional QCMs (Ogi *et al.* (2008a)). Since the nonspecific adsorption usually causes a small change in the resonance frequency, a highly sensitive QCM is required. The mass sensitivity of our 55 MHz QCM is 0.14 ng/(cm^2Hz), which is much better than that of the conventional 5 MHz QCM ($\sim$17 ng/(cm^2Hz)) by a factor larger than 100. The WE-QCM also allows the affinity measurement of target molecules on the naked α-SiO_2 surface. Few biosensors make this task possible because conventional QCM and SPR chips need metallic coatings on their surfaces. The

lateral-field exited acoustic-wave biosensors will be another candidate because they do not need a metallic electrode on the sensing region (Hu *et al.* (2004)). Both α-SiO_2 and the amorphous SiO_2 glass consist of the SiO_4 tetrahedral unit (Tarumi *et al.* (2007)) and we can expect similar nonspecific binding properties of proteins on them.

2 Experimental Section

2.1 Measurement system

30-μm-thick AT-cut quartz plates with a 3-mm diameter are used throughout this study. Their fundamental resonance frequencies of the pure thickness shear vibration are near 55 MHz. The quartz plate is fixed in the sensor cell (Ogi *et al.* (2006a)) located in the temperature control box in the homebuilt flow-injection system (Ogi *et al.* (2008a)). The micropump (Uniflows Co. Ltd., Model 3005FSB2) (not shown) makes a steady flow of the carrier solution of phosphate-buffer solution (PBS) with pH 7.4. We select an analyte to be injected by the switching valve (FLOM Co., Ltd., Model 401) (not shown) among eight vials. Before the micropump, the solution flows in the degasifier (Uniflows Co. Ltd., Model DG-7101) (not shown) and in a 3-m-long Teflon tube column, which maintains the solution temperature at 25 °C. The solution then enters into the QCM cell and flows along both surfaces of the sensor chip. (The WE-QCM can use both surfaces as the sensing region.) The antenna set outside the cell measures the resonance frequency of the quartz plate with the noncontacting manner. The driving burst signal is applied to the generation antenna to cause the thickness-shear vibration (Ogi *et al.* (2006b, 2008c)). After the

excitation, the detection antenna receives the reverberation signals, which are fed to a superheterodyne spectrometer (RITEC Inc., Model SNAP-1-100) to measure the phase and amplitude of the received signals using the driving signal as the reference (Hirao and Ogi (2003)). The resonance frequency is obtained from the peak-amplitude frequency. We repeat the frequency scan until the resonance frequency becomes sufficiently stable. Then we monitor the phase shift at the fixed frequency to make a quick measurement ($\sim$0.1 s). The frequency change is determined from the linear relationship between frequency and phase at the resonance (Ogi *et al.* (2008a)).

2.2 Sensor Chip Preparation

We prepared five kinds of sensor chips as follows.

(i) A naked quartz plate. It was cleaned in a piranha solution (98%H_2SO_4:33%H_2O_2=7:3) and rinsed with ultrapure water. It was then set in the QCM cell. We denote this chip as SiO_2.

(ii) A quartz plate covered by Au thin films. We deposited 2-nm-thick Cr/18-nm-thick Au films on both surfaces of the quartz plate. The undercoating Cr films were used to make the adhesion between quartz and Au tighter. The sensor chip was cleaned by the piranha solution, rinsed with the ultrapure water, and installed in the QCM cell. We denote this chip as Au/SiO_2.

(iii) A quartz plate covered by PEG. We used an NH_2-PEG, which has the amino-terminal end and the hydroxyl terminal end at the other side. The NH_2-PEGs were immobilized on the quartz plate through the self-assembled monolayer (SAM) on the Au film. After the deposition of the Au thin films, the sen-

sor chip was cleaned in the piranha solution, rinsed with the ultrapure water, and immersed in a 10 mM 10-carboxy-1-decanethiol/absolute ethanol solution for 20 h at 4°C. After rinsing with the absolute ethanol, the sensor chip was immersed in a 100-mM EDC (1-ethyl-3-(3-dimethylaminopropyl)carbodiimide, hydrochloride) solution for 1 h to activate the carboxyl terminals, and it was immersed in a 10 mg/ml NH_2-PEG/PBS solution, containing 100 mM sulfo-NHS (N-hydroxysulfosuccinimide sodium salt) as well, for 12 h. Activated carboxyl terminals of the SAM and amino terminals of the NH_2-PEG bind covalently to cover the sensor surfaces with the PEG. We denote this chip as PEG/SAM/Au/SiO_2.

(iv) A quartz plate covered by BSA. BSA molecules were immobilized on the SAM with the same procedure as that used in producing the PEG/SAM/Au/SiO_2 chip. The SAM-coated sensor chip was activated by EDC and was immersed in a 10 mg/ml BSA/PBS solution, containing 100 mM sulfo-NHS, to cover its surfaces with BSA covalently. We denote this chip as BSA/SAM/Au/SiO_2.

(v) A quartz plate covered by SPA. We fabricated this chip to compare the specific and nonspecific adsorption behavior of hIgG. It is well known that SPA and hIgG show the specific binding with a high affinity (Hanson and Shumaker (1984)). The SAM-coated sensor chip was activated by EDC and was immersed in a 400 μg/ml SPA/PBS solution, containing 100 mM sulfo-NHS, to cover its surfaces with SPA. We denote this chip as SPA/SAM/Au/SiO_2.

We independently study nonspecific adsorption abilities of the four materials (hIgG, SPA, PEG, and BSA) on SiO_2, Au/SiO_2, PEG/SAM/Au/SiO_2, and BSA/SAM/Au/SiO_2. As the analyte, we used a standard PEG with hydroxy ends (molecular weight is 6 kDa). The concentration of the injected protein

is between 10 and 100 μg/ml. Also, we compare the nonspecific and specific binding behavior of hIgG on the five sensor chips.

hIgG was obtained from Athens Research and Technology, Inc. (product num. 16-16-090707; purity ∼95%). SPA was from Zymed Laboratories, Inc. (product num. 10-1100; purity ∼98%). BSA (No. 9048-46-8) was from Sigma-Aldrich Japan. Hydroxy-end PEG (product num. PEG 6000 (33137)) was from Serva Electrophoresis. NH_2-PEG (O-(2-Aminoethyl)polyethylene glycol) was from Sigma-Aldrich Japan (product num. 07969). SAM (10-carboxy-1-decanethiol (product num. C385)) and EDC (product num. W001) were from Dojindo Laboratories. Sulfo-NHS was from Sigma-Aldrich Japan (product num. 56485). All of other chemical substances were purchased from Wako Pure Chemical Industries Ltd.

2.3 Kinetics analysis

The frequency change Δf is caused by the addition of the target mass Δf_{mass} (Sauerbrey (1959)) and also by the viscosity change at the sensor surface Δf_{visco} (Kanazawa and Gordon (1985); Martin *et al.* (1991)):

$$-\Delta f = \Delta f_{mass} + \Delta f_{visco} \tag{1}$$

where

$$\Delta f_{mass} = 2N \frac{(\Delta m/A_e)}{\sqrt{\mu_q \rho_q}} \frac{A_e}{A_q} \cdot f_1^2 \tag{2}$$

$$\Delta f_{visco} = \sqrt{N} \frac{\Delta\left(\sqrt{\rho_f \eta_f}\right)}{\sqrt{\pi \rho_q \mu_q}} \cdot f_1^{\frac{3}{2}}. \tag{3}$$

Here, integer N denotes the overtone number, f_1 the fundamental resonance frequency, and Δm the mass adsorbed on the sensor surfaces. A_e and A_q are the effective sensing area and the area of the crystal surface, respectively. Their ratio A_e/A_q is smaller than 1 for a conventional QCM using a single side of the quartz plate, but it almost equals 2 in the present study because both surfaces are active for sensing. ρ_q and μ_q are the mass density and the shear modulus of the AT-cut quartz, and ρ_f and η_f are effective mass density and viscosity caused by the interaction between the surrounding liquid and the adsorbed film layer. In recent low-frequency QCM measurements, the change in internal friction of the resonator system ΔD has been measured as well as the frequency change for making quantitative discussion possible (Höök *et al.* (1998); Rodahl *et al.* (1995)). However, equations (1)-(3) indicate that the higher frequency we use, the less significant the frequency change caused by the viscosity effect becomes, compared with the mass-loading effect. Indeed, the viscosity effect can be estimated as follows. During the adsorption of the target molecules, the term $\sqrt{\rho_f \eta_f}$ increases to cause the frequency decrease Δf_{visco}. In a simple spring-dashpot model with no sliding of the adoption layer, the damping term is associated with the internal-friction change as (Rodahl and Kasemo (1996))

$$\Delta\left(\sqrt{\rho_f \eta_f}\right) = \frac{1}{2}\sqrt{\frac{N}{f_1}}\sqrt{\pi \rho_q \mu_q}\Delta D \tag{4}$$

For example, Δf value was about -60 Hz when a 0.15 μM ferritin solution was injected in a 5 MHz QCM system, accompanying the damping change of $\Delta D \sim 10^{-6}$ (Höök *et al.* (1998)). This observation and Eqs. (2)-(4) allow the estimation of the ratio of $\Delta f_{visco}/\Delta f_{mass}$; this value equals 0.013 for the 55 MHz QCM, indicating negligible viscosity effect in a high-frequency QCM.

Therefore, we neglected the viscosity effect in this study.

In order to evaluate the adsorption ability, we determine the equilibrium constant K_A and the number density of effective binding sites on the sensor chip. Assuming that the nonspecific binding occurs with a pseudo-first-order manner and that the Sauerbrey equation (Eq. (2)) applies, the reaction kinetics yields the change in the site number σ_{site} per unit effective area during the binding reaction (Eddowes (1987); Liu *et al.* (2003b))

$$\sigma_{site} = \frac{k_a C_A}{k_a C_A + k_d} \sigma^0_{site} \left[1 - \mathrm{e}^{-(k_a C_A + k_d)t}\right] \tag{5}$$

Here, k_a and k_d are the association rate constant and the dissociation rate constant, respectively. σ^0_{site} denotes the total number density of binding sites on the effective area for the analyte. C_A is the concentration of the analyte. Because the mass change is expressed by $\Delta m = A_e \sigma_{site} p_A / N_A$, where p_A and N_A are molecular weight of the analyte and the Avogadro constant, respectively, the frequency change becomes from Eq. (2) as

$$\Delta f = -\frac{4 f_1^2}{\sqrt{\rho_q \mu_q}} \frac{p_A}{N_A} \sigma_{site} \tag{6}$$

Here we used A_e/A_q=2. Therefore, the total number density σ^0_{site} of the binding site on effective surface is given by

$$\sigma^0_{site} = \frac{\sqrt{\rho_q \mu_q}}{4 f_1^2} \frac{N_A}{p_A C_A k_a} \left(\frac{d\Delta f}{dt}\right)_{t=0} \tag{7}$$

We determined the slope of the frequency change $\left(\frac{d\Delta f}{dt}\right)_{t=0}$ at the beginning of the reaction (t=0).

From Eqs .(5) and (6), the frequency changes exponentially with the exponential coefficient

$$\alpha = k_a C_A + k_d \tag{8}$$

and we obtain the kinetics constants k_a and k_d, and then their ratio $K_A = k_a/k_d$ (Ebara *et al.* (1996)) from the relationship between C_A and α. We thus determined the equilibrium constant K_A and the total site number density σ^0_{site} from the binding curves with different concentrations. The affinity analysis using the exponential coefficient has the advantage that it is independent on the amount of the frequency change, but on the kinetics constants and the analyte concentration. The amount of the frequency change highly depends on the surface condition, and it will be fluctuated in the low-affinity bindings of the nonspecific adsorption.

3 Results and Discussions

Note that among the adsorption systems studied here, only the SPA and hIgG pair causes the specific binding, and the other pairs interact with the nonspecific bonds. We first discuss the nonspecific adsorption ability. Figures 1(a)-(d) show typical binding curves for the nonspecific adsorption of the materials on the four sensor chips when 10 μg/ml analyte solutions were injected. hIgG, SPA and BSA show significant nonspecific adsorption on the SiO_2 and Au surfaces. Especially, the adsorption ability of SPA on SiO_2, and that of BSA on Au are remarkable. On the other hand, PEG shows much less binding activity on them. Both PEG and BSA show very poor binding abilities with hIgG.

PEG and SPA show unusual adsorption behaviors on the Au surfaces (Fig. 1(b)). The frequency decreases markedly at first, but it recovers quickly. It then gradually decreases. Therefore, a short-time adsorption and dissociation occurs before the steady adsorption process. This behavior was well reproducible for the SPA-Au and PEG-Au pairs. However, we have not clarified the mechanism at present, which will be involved in our future work.

The amount of frequency decrease in Fig. 1 depends on the molecular mass of the analyte, binding affinity, and the number of binding sites on the sensor chip. Therefore, we cannot evaluate the binding ability only from the frequency response obtained for a single-concentration analyte. We then determined the equilibrium constant and the number density of binding sites from the binding curves with different concentrations of the analyte (Ogi *et al.* (2008a)). The result is shown in Fig. 2. The error bars indicate the standard deviation of the values obtained from three independent measurements. (We fabricated the sensor chip in each measurement.) The large error bars ($>\sim$50%) are caused by the low reproducibility of the nonspecific adsorption behavior. However, we can see significant differences among the determined constants of the different nonspecific adsorption systems, exceeding the error bar. The hIgG-Au pair shows the highest K_A value (K_A =1.3$\times 10^7$ M^{-1}) despite the small number of binding sites. Thus, when Au films are used in a biosensor system, they have to be completely covered with appropriate blocking materials; otherwise antibodies will be adsorbed tightly. hIgG also shows high affinity with the SiO_2 surface (K_A =4.2$\times 10^6$ M^{-1}) and the number of binding sites is also large. This suggests that in a flow-injection system using glass-like materials, the nonspecific binding of antibodies with the glass walls will occur, and the concentration of the analyte will be lowered. We note that SPA adsorbs on

all surfaces with high affinities of $K_A \sim 10^6 M^{-1}$, regardless of the observation that no significant frequency changes occur on PEG and BSA surfaces in Fig. 1. This is attributed to small number of the binding sites on the PEG and BSA surfaces for SPA. An SPA molecule tightly binds with the PEG and BSA surfaces, but the small number of binding sites restricts the frequency change.

PEG shows very low affinities for SiO_2 (K_A =4.3×10^4 M^{-1}) and Au (K_A =6.6×10^4 M^{-1}) surfaces, whereas BSA shows high affinities for them, especially for the SiO_2 surface (K_A =1.4×10^6 M^{-1}). Therefore, BSA can be a candidate coating material to cover the inner surfaces of a biosensor flow system.

Figures 1(c) and (d) indicate that both PEG and BSA work as the blocking materials for hIgG because they show low affinities for hIgG with K_A =1.4×10^4 and 1.5×10^4 M^{-1}, respectively. However, the number of binding sites is much larger on PEG than on BSA, which is associated with the smaller molecular size of PEG. When the affinity value is identical, a small number of binding sites is preferable. Thus, BSA is better blocking material than PEG in the case of hIgG. Figure 3 confirms this view; it compares the specific and nonspecific binding of hIgG on the five QCM chips. Because SPA and hIgG show the specific binding with a much higher affinity ($K_A \sim 10^8 - 10^9$ M^{-1}) (Hanson and Shumaker (1984); Ogi *et al.* (2007a)), the largest change in the resonance frequency occurs. hIgG binds with other surfaces slightly except for BSA. The frequency remained nearly unchanged during the flow of the hIgG solution when the sensor surfaces were covered by BSA, confirming the high-blocking ability of BSA for hIgG.

4 CONCLUSION

Using the homebuilt wireless-electrodeless 55 MHz QCM system, we quantitatively evaluated nonspecific adsorption of proteins on PEG and BSA as well as Au and SiO_2 surfaces. hIgG molecule adsorbs on Au and SiO_2 surfaces with high affinity values. Especially, nonspecific binding between hIgG and Au surface is significant, where the K_A value is on the order of 10^7 M^{-1}. PEG shows low affinities for Au and SiO_2 surfaces, whereas BSA shows high affinities with them. SPA shows relatively high affinities on all surfaces. BSA and PEG show nearly identical blocking abilities to hIgG, but the number of binding sites on PEG is much larger, indicating that BSA is more favorable blocking material for IgG-related biosensors. This was confirmed by comparing the specific binding behavior between SAP and hIgG with the nonspecific binding between BSA and hIgG.

References

Drouvalakis, K. A., Bangsaruntip, S., Hueber, W., Kozar, L. G., Utz, P. J., Dai, H., 2008. Biosens. Bioelectron. 23, 1413-1421.

Ebara, Y., Itakura, K., Okahata, Y., 1996. Langmuir. 12, 5165-5170.

Eddowes, M. J., 1987. Biosensors. 3, 1-15.

Edvardsson, M., Svedhem, S., Wang, G., Richter, R., Rodahl, M., Kasemo, B., 2009. Anal. Chem.. 81, 349-361.

Hanson, D. C., Schumaker, V. N., 1984. J. Immunol. 132, 1397-1409.

Hirao, M., Ogi, H., 2003. EMATs for Science and Industry: Noncontacting Ultrasound Measurements (Springer-Kluwer, Boston).

Höök, F, Rodahl, M., Brzezinski, P., B. Kasemo, B., 1998. Langmuir 14, 729-734.

Hu, Y., French, L.A. Jr., Radecsky, K., da Cunha, M.P., Millard, P., Vetelino, J.F., 2004. IEEE Trans. Ultrason. Ferroelectr. Freq. Control. 51, 1373-80.

Kanazawa, K. K., Gordon, J. G., 1985. Anal. Chim. Acta. 175, 99-105.

Kang, H., Muramatsu, H., 2009. Biosens. Bioelectron. 24, 1318-1323.

Liu, Y., Yu, X., Zhao, R., Shangguan, D., Bo, Z., Liu, G., 2003a. Biosens. Bioelectron. 18, 1419-14279.

Liu, Y., Yu, X., Zhao, R., Shangguan, D., Bo, Z., Liu, G., 2003b. Biosens. Bioelectron. 19, 9-19.

Martin, S. J., Granstaff, V. E., Frye, G. C., 1991. Anal. Chem. 63, 2272-2281.

Muramatsu, H., Dicks, M. D., Tamiya, E., Karube, I., 1987. Anal. Chem. 59, 2760-2763.

Ogi, H., Motohisa, K., Matsumoto, T., Hatanaka, K. Hirao, M., 2006a. Anal Chem. 78, 6903-6909.

Ogi, H., Niho, H., Hirao, M., 2006b. Appl. Phys. Lett. 88, 141110.

Ogi, H., Motohisa, M., Hatanaka, K., Ohmori, T., Hirao, M., Nishiyama, M., 2007a. Biosens. Bioelectron. 22, 3238-3242.

Ogi, H., Motohisa, K., Hatanaka, K., Ohmori, T., Hirao, M., Nishiyama, M., 2007b. Jpn. J. Appl. Phys. 46, 4693-4697.

Ogi, H., Fukunishi, Y., Omori, T., Hatanaka, K., Hirao, M., Nishiyama, M., 2008a., Anal. Chem. 80, 5494-5500.

Ogi, H., Ohmori, T., Hatanaka, K., Hirao, M., Nishiyama, M., 2008b. Jpn. J. Appl. Phys. 47, 4021-4023.

Ogi, H., Inoue, T., Nagai, H., Hirao, M., 2008c. Rev. Sci. Instrum. 79, 053701.

Rodahl, M., Höök, F, Krozer, A., Brzezinski, P., 1995. Rev. Sci. Instrum. 66, 3924-3930.

Rodahl, M., Kasemo, B., 1996. Sens. Actuat. 54, 448-456.

Sauerbrey, G., 1959. Z. Phys. 155, 206-222.

Senaratne, W., Takada, K., Das, R., Cohen, J., Baird, B., Abruna, H. D., Ober, C. K., 2006. Biosens. Bioelectron. 22, 63-70.

Shen, Z., Huang, M., Xiao, C., Zhang, Y., Zeng, X., Wang, P. G., 2007. Anal. Chem. 79, 2312-2319.

Shu, W., Laurenson, S., Knowles, T. P. J., Ferrigno, P. K., Seshia, A. A., 2008. Biosens. Bioelectron. 24, 233-237.

Suprun, E., Shumyantseva, V., Bulko, T., Rachmetova, S., Rad'ko, S., Bodoev, N., Archakov, A., 2008. Biosens. Bioelectron. 24, 825-830.

Tarumi, R., Nakamura, K., Ogi, H., Hirao, M., 2007. J. Appl. Phys. 102, 113508.

Wąsowicz, M., Viswanathan, S., Dvornyk, A., Grzelak, K., K?udkiewicz, B., Radecka, H., 2008. Biosens. Bioelectron. 24, 284-289.

Wang, T., Muthuswamy, J., 2009. Anal. Chem. 80, 8576-8582.

Figure Caption

Fig. 1 (Color)Typical frequency changes observed during the nonspecific adsorption of BSA, PEG, hIgG and SPA on (a) SiO_2, (b) Au, (c) PEG, and (d) BSA when the concentration of the analyte was 10 μg/ml.

Fig. 2 The equilibrium constant K_A and the total number density of binding sites σ^0_{site} for various pairs among the proteins and surfaces.

Fig. 3 Comparison of the adsorption behavior of hIgG on the five sensor chips, where the specific adsorption between hIgG and SPA is involved. The arrow below PBS represents the time when the buffer solution is injected after the hIgG solution, causing the dissociation reaction between hIgG and SPA.

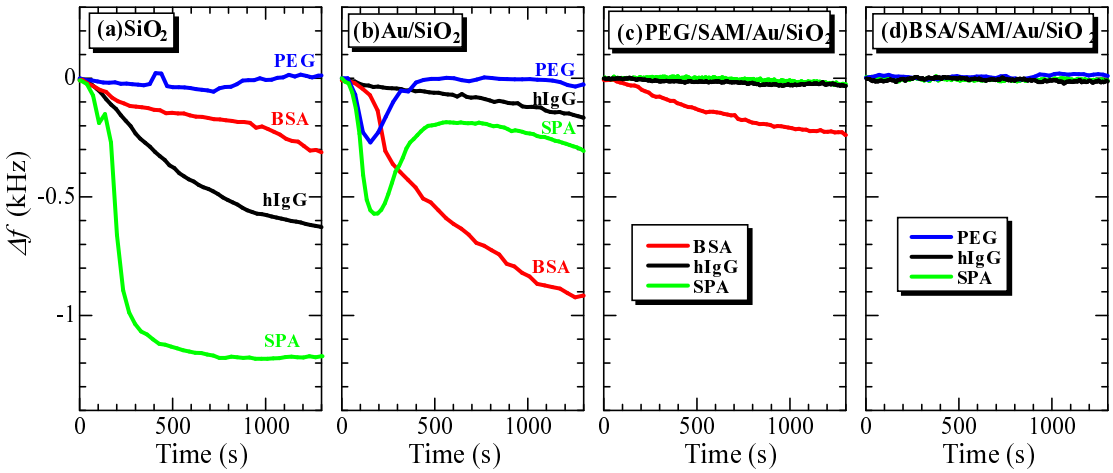
(a)SiO2
(b)Au/SiO2
(c)PEG/SAM/Au/SiO2
(d)BSA/SAM/Au/SiO2
PEG
BSA
hIgG
SPA
Δf (kHz)
0
-0.5
-1
0
500
1000
Time (s)

Fig. 1.

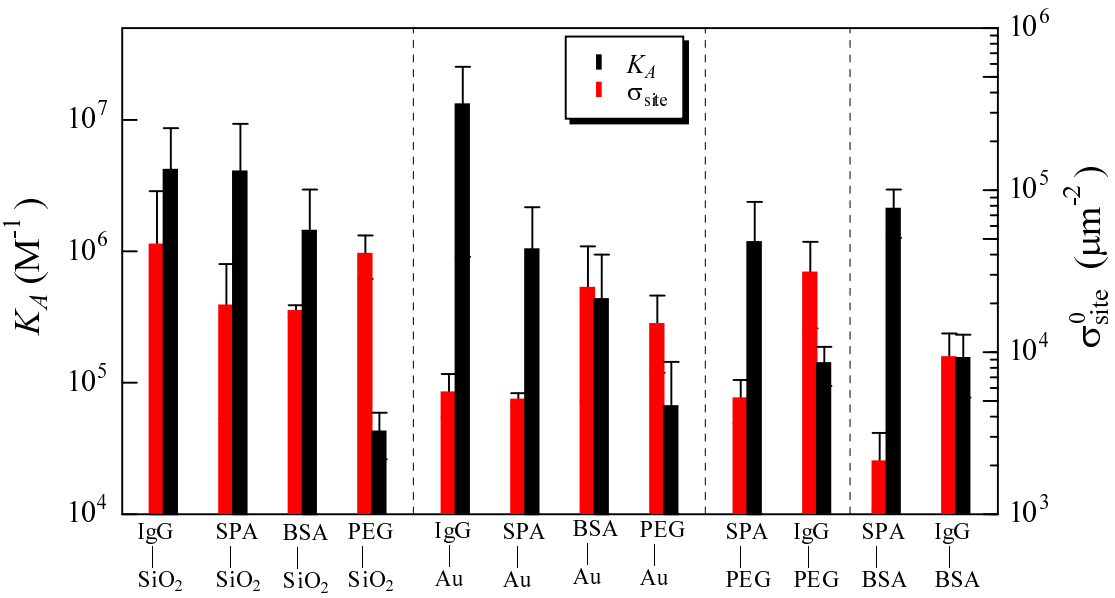
K_A
σ_{site}
K_A (M^{-1})
σ^0_{site} (μm^{-2})
10^7
10^6
10^5
10^4
10^6
10^5
10^4
10^3
IgG
SPA
BSA
PEG
IgG
SPA
BSA
PEG
SPA
IgG
SPA
IgG
SiO_2
SiO_2
SiO_2
SiO_2
Au
Au
Au
Au
PEG
PEG
BSA
BSA

Fig. 2.

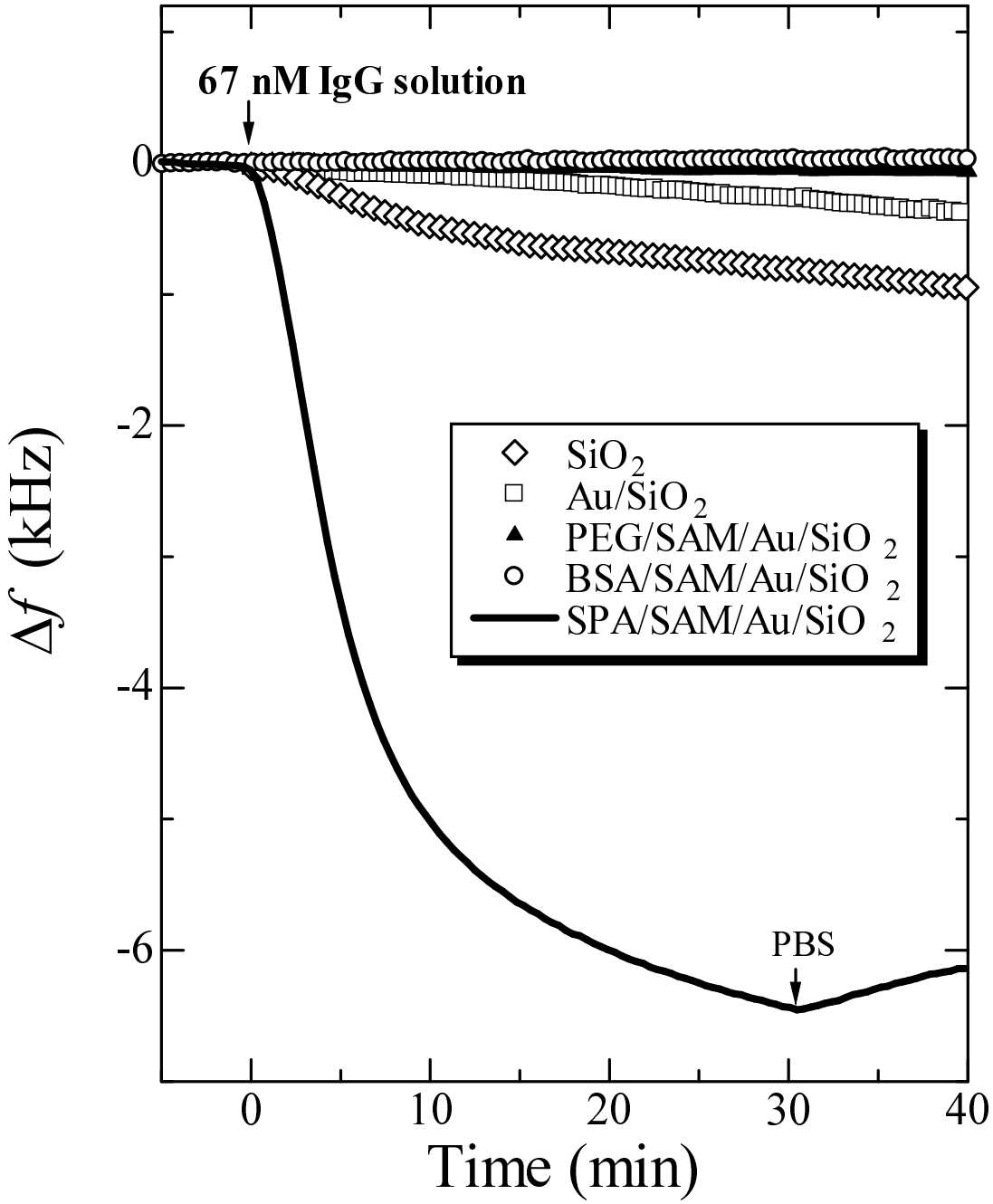
67 nM IgG solution
0
-2
-4
-6
Δf (kHz)
SiO2
Au/SiO2
PEG/SAM/Au/SiO2
BSA/SAM/Au/SiO2
SPA/SAM/Au/SiO2
PBS
0
10
20
30
40
Time (min)

Fig. 3.